Detecting photon-photon interactions in a superconducting circuit

Li-Jing Jin,[1,2,*] Manuel Houzet,[3,4] Julia S. Meyer,[3,4] Harold U. Baranger,[5] and Frank W. J. Hekking[1,2]

[1]*Université Grenoble Alpes, LPMMC, F-38000 Grenoble, France*
[2]*CNRS, LPMMC, F-38000 Grenoble, France*
[3]*Université Grenoble Alpes, INAC-SPSMS, F-38000 Grenoble, France*
[4]*CEA, INAC-SPSMS, F-38000 Grenoble, France*
[5]*Department of Physics, Duke University, Durham, North Carolina 27708-0305, USA*

A local interaction between photons can be engineered by coupling a nonlinear system to a transmission line. The required transmission line can be conveniently formed from a chain of Josephson junctions. The nonlinearity is generated by side-coupling this chain to a Cooper pair box. We propose to probe the resulting photon-photon interactions via their effect on the current-voltage characteristic of a voltage-biased Josephson junction connected to the transmission line. Considering the Cooper pair box to be in the weakly anharmonic regime, we find that the dc current through the probe junction yields features around the voltages $2eV = n\hbar\omega_s$, where ω_s is the plasma frequency of the superconducting circuit. The features at $n \geqslant 2$ are a direct signature of the photon-photon interaction in the system.

I. INTRODUCTION

Creating strong light-matter interaction attracts increasing attention due to both fundamental reasons [1–4] and its potential application in quantum communication science [1,5,6]. A prototypical system for studying that interaction consists of a quantum system inside a photonic cavity [7]. However, recent rapid experimental advances in several areas [8–13] have focused attention on *one-dimensional* systems in which the quantum system is embedded in a waveguide or transmission line. In the absence of coupling, photons propagate freely down the line. A coupling between the quantum system and the line generates an effective photon-photon interaction that causes correlations among the photons. This has led to, for instance, the prediction of Kondo physics [14], antibunching resulting from a photon-blockade effect [15,16], inelastic photon scattering [15,17,18], giant Kerr nonlinearities [19], and entanglement among photons of different frequencies in the line [20].

The strength of the coupling between the local quantum system and the transmission line has been studied theoretically in detail in the Ohmic spin-boson model, which consists of a single two-level system (the spin) bilinearly coupled to the photons in the line (the bosons). It was shown [21,22] that the coupling parameter is set by the ratio of the line impedance, Z, to the quantum of resistance, $R_Q = h/(2e)^2 \approx 6.45$ kΩ. The impedance of typical transmission lines is of order the vacuum impedance, $Z_{\text{vac}} \approx 377$ Ω, thereby allowing only weak coupling.

Superconducting circuits are a promising platform for exploring strong-coupling phenomena, and, indeed, the first experiments observing such phenomena have appeared [23,24]. One benefit of using superconducting circuits is that a chain of Josephson-coupled superconducting islands acts as a transmission line with a large tunable impedance $Z \lesssim R_Q$, which is only limited by the superconductor/insulator transition [25].

Recent experiments have studied the microwave properties of such Josephson junction chains [26–29]. Moreover, superconducting circuits allow the realization of a variety of quantum systems that behave like artificial atoms [1,30].

In our work, we take the quantum system coupled to the transmission line to be a Cooper pair box [31,32]. Then, we propose to detect the photon-photon interaction generated by that system by measuring the dc current-voltage characteristic of an additional Josephson junction connected to the transmission line. According to dynamical Coulomb blockade theory [also called $P(E)$ theory] [33], Cooper pairs can tunnel incoherently through that probe junction provided that they can release their energy $2eV$ into the environment, which in our case consists of the transmission line with the side-coupled circuit. Therefore, the dc current reflects both the elastic and inelastic scattering properties of photons.

Let us consider the current-voltage characteristic in more detail: In the harmonic regime, the effective impedance of the environment is almost flat, except at frequencies near the plasma frequency ω_s of the superconducting side circuit (the Cooper pair box). This results in a feature at $2eV = \hbar\omega_s$ in the current-voltage characteristic. Anharmonic corrections cause additional features near the voltages $2eV = n\hbar\omega_s$ ($n \geqslant 2$ integer) through inelastic photon scattering. These additional features are most pronounced in the strong-coupling regime when Z approaches R_Q ($Z \lesssim R_Q$).

The paper is organized as follows. In Sec. II, we introduce the Hamiltonian that describes the circuit studied. The current-voltage characteristic of the probe junction in the harmonic regime is calculated in Sec. III. In Sec. IV, we include a weak anharmonic correction and study the effect of the resulting photon-photon interaction on the current. Finally, we conclude in Sec. V.

II. THE CIRCUIT STUDIED

We are interested in the interactions of photons propagating in a nonlinear electromagnetic environment. In particular, we study a transmission line, consisting of a chain of Josephson

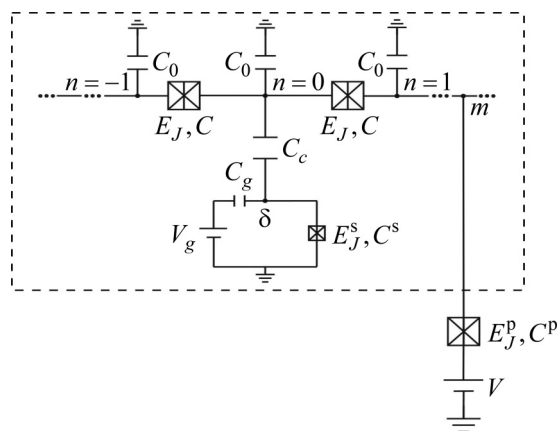————
*li-jing.jin@lpmmc.cnrs.fr

FIG. 1. The system consists of a transmission line that is capacitively coupled (capacitor C_c) to a Josephson junction, shown inside the dashed box. The transmission line is realized using a chain of Josephson junctions with Josephson energy E_J much larger than the charging energy E_C. The system is probed at node m using another Josephson junction (outside the dashed box) whose current-voltage characteristic is sensitive to the properties of the system.

junctions, to which an additional Josephson junction acting as the nonlinear element is side-coupled at node $n = 0$ as shown in Fig. 1 (dashed box). We assume weak coupling; namely the coupling capacitance, C_c, is much smaller than the characteristic capacitances of the chain and the nonlinear element.

The Hamiltonian of the system is, thus, assembled from three parts,

$$H = H_T + H_J + H_c, \qquad (1)$$

where H_T is the Hamiltonian of the transmission line, H_J is the Hamiltonian of the side-coupled Josephson junction, and H_c is the coupling Hamiltonian.

A transmission line with large impedance can be realized using a chain of Josephson junctions in the limit where the Josephson energy E_J is much larger than the charging energy E_C [26,27]. The chain is described by the charge and phase operators at each node n, denoted Q_n and ϕ_n, respectively. They are conjugate variables satisfying the commutation relation $[Q_n, \phi_m] = -2ie\delta_{nm}$. As $E_J \gg E_C$, phase fluctuations are small and we may approximate the Josephson coupling by a quadratic term. We further consider the case where the capacitance to the ground C_0 is much larger than the mutual capacitance C. Then, for frequencies much smaller than the plasma frequency of Josephson junctions in the chain, the Hamiltonian takes the simple form [25]

$$H_T = \sum_n \left[\frac{Q_n^2}{2C_0} + \frac{1}{(2e)^2} \frac{(\phi_n - \phi_{n+1})^2}{2L} \right], \qquad (2)$$

where the inductance is $L = 1/(4e^2 E_J)$. Note that we use units where $\hbar = 1$. At frequencies $\omega \ll \omega_0$, where $\omega_0 \equiv 1/\sqrt{LC_0}$, the transmission line has a linear spectrum.

The side-coupled Josephson junction with Josephson energy E_J^s is described by the Hamiltonian

$$H_J = \frac{(Q_\delta + C_g V_g)^2}{2C_\Sigma} - E_J^s \cos \phi_\delta, \qquad (3)$$

where Q_δ and ϕ_δ are the conjugate charge and phase operators at node δ (see Fig. 1). Furthermore, C_g and V_g are the gate capacitance and gate voltage, respectively, and $C_\Sigma = C^s + C_g$ is the total capacitance of the side-coupled Josephson junction.

Finally, we turn to the coupling Hamiltonian H_c. When the coupling capacitance is small, $C_c \ll C_0, C_\Sigma$, the coupling Hamiltonian reads

$$H_c = \frac{C_c}{C_0 C_\Sigma} Q_0 (Q_\delta + C_g V_g), \qquad (4)$$

where we used the fact that for $C \ll C_0$ the coupling is local; i.e., the side-coupled Josephson junction couples only to the charge Q_0 at $n = 0$. The Hamiltonian H fully describes our nonlinear system.

As a next step, we introduce the probe circuit used to characterize the photon-photon interactions generated by the nonlinear system. The probe circuit consists of yet another Josephson junction, with Josephson energy E_J^p and in series with a voltage source as shown in Fig. 1, coupled to the transmission line at node m [34,35]. The current-voltage characteristic of the probe Josephson junction is influenced by the correlations of the phase $\phi_m(t)$ at node m, correlations that depend on the fluctuations in the nonlinear environment. The I-V characteristic may, thus, be used to characterize the photon-photon interactions in the nonlinear system.

In particular, using $P(E)$ theory, it can be shown that at zero temperature the current flowing through the probe Josephson junction takes the form [33]

$$I(V) = \pi e \left(E_J^p\right)^2 P(2eV), \qquad (5)$$

for voltages $eV < 2\Delta$, where Δ is the superconducting gap, and

$$P(E) = \frac{1}{2\pi} \int_{-\infty}^{\infty} dt \, e^{iEt} \langle e^{i\phi_m(t)} e^{-i\phi_m(0)} \rangle_{H_{env}} \qquad (6)$$

is the probability of the probe Josephson junction to emit energy E to its environment, described by the Hamiltonian H_{env}. Though $P(E)$ theory is usually presented in the context of a linear environment (H_{env} is assumed to be quadratic) [33,36–38], Eqs. (5) and (6) hold more generally for a nonlinear environment [34]. If the capacitance of the probe Josephson junction is sufficiently small, $C^p \ll C_0$, the Hamiltonian of the environment in Eq. (6) may be replaced by the Hamiltonian H of the nonlinear system we want to characterize. Our task is then to compute the phase correlator $\langle e^{i\phi_m(t)} e^{-i\phi_m(0)} \rangle_H$.

III. THE LINEAR REGIME

As a first step, we will consider the system in the linear regime, where photons do not interact. That is, we assume $E_J^s \gg e^2/(2C_\Sigma)$ and approximate the junction Hamiltonian H_J in Eq. (3) by

$$H_J^{(0)} = \frac{(Q_\delta + C_g V_g)^2}{2C_\Sigma} + \frac{E_J^s}{2} \phi_\delta^2. \qquad (7)$$

In this section, we study the behavior of this simplified system described by $H^{(0)} = H_T + H_J^{(0)} + H_c$ to set the basis for investigating interaction effects, the main focus of our work, in the following section. In this regime, the gate voltage V_g can be gauged out of the Hamiltonian, and the side-coupled

circuit behaves as a harmonic oscillator with plasma frequency $\omega_s \equiv 2e\sqrt{E_J^s/C_\Sigma}$. We will assume that $\omega_s \ll \omega_0$.

A. Phase-phase correlator

As the system is noninteracting, the phase-phase correlation function in Eq. (6) can be simplified by exploiting Wick's theorem [33]:

$$\langle e^{i\phi_m(t)}e^{-i\phi_m(0)}\rangle_{H^{(0)}} = e^{J(t)}, \quad (8)$$

where

$$J(t) \equiv \langle[\phi_m(t) - \phi_m(0)]\phi_m(0)\rangle_{H^{(0)}}. \quad (9)$$

To evaluate the correlator, we use the retarded Green's function $G_R^{(0)}(\phi_n,\phi_m;t) = i\Theta(t)\langle[\phi_n(t),\phi_m(0)]\rangle_{H^{(0)}}$, where $\Theta(t)$ is the Heaviside step function. The relation between the two is most easily written in frequency space. At zero temperature, it reads

$$\langle\phi_n(t)\phi_n(0)\rangle_{H^{(0)}} = 2\int_0^\infty \frac{d\omega}{2\pi}e^{-i\omega t}\,\text{Im}[G_R^{(0)}(\phi_n,\phi_n;\omega)]. \quad (10)$$

The local Green's function $G_R^{(0)}(\phi_m,\phi_m;\omega)$ needed to compute $J(t)$ is obtained by deriving its equation of motion and using scattering theory (see Appendix A). Photons propagate freely in the transmission line and are scattered by the side-coupled harmonic oscillator at node $n = 0$, yielding the reflection coefficient

$$r(\omega) = -\left[1 - 2i\frac{\omega_0}{\omega}\left(1 + \frac{C_0 C_\Sigma}{C_c^2}\frac{\omega^2 - \omega_s^2}{\omega^2}\right)\right]^{-1}. \quad (11)$$

In terms of this reflection coefficient, the Green's function is

$$G_R^{(0)}(\phi_m,\phi_m;\omega) = i\frac{\pi}{\omega}\frac{Z_0}{R_Q}\left[1 + r(\omega)e^{2i\frac{\omega}{\omega_0}m}\right], \quad (12)$$

where $Z_0 = \sqrt{L/C_0}$ is the impedance of the chain. Under the conditions specified above, $C_0 C_\Sigma/C_c^2 \gg 1$ and $\omega_s \ll \omega_0$, the reflection coefficient has a narrow resonance at $\omega = \omega_s$ with width

$$\Gamma = \frac{1}{4}\frac{C_c^2}{C_0 C_\Sigma}\frac{\omega_s}{\omega_0}\omega_s. \quad (13)$$

Close to the resonance, we can approximate Eq. (11) as $r(\omega) = -1/[1 - i(\omega - \omega_s)/\Gamma]$.

Substituting Eq. (10) into Eq. (9) and using the Green's function (12), one obtains

$$J(t) = \frac{2}{R_Q}\int_0^\infty \frac{d\omega}{\omega}\text{Re}[Z(\omega)](e^{-i\omega t} - 1), \quad (14)$$

as expected from $P(E)$ theory [33], with the impedance

$$Z(\omega) = \frac{Z_0}{2}\left[1 + r(\omega)e^{2i\frac{\omega}{\omega_0}m}\right]. \quad (15)$$

The prefactor $1/2$ corresponds to the fact that the probe junction "sees" an environment consisting of *two* half-infinite transmission lines. Far from the resonance at ω_s, the impedance is unaffected by the side-coupled Josephson junction as $r(\omega) \to 0$. In contrast, at the resonance, photons are strongly scattered. In particular when the probe and the scatterer are coupled to the same node ($m = 0$), $r(\omega_s) = -1$ so that transport is completely blocked due to destructive interference. Changing the distance between the probe and
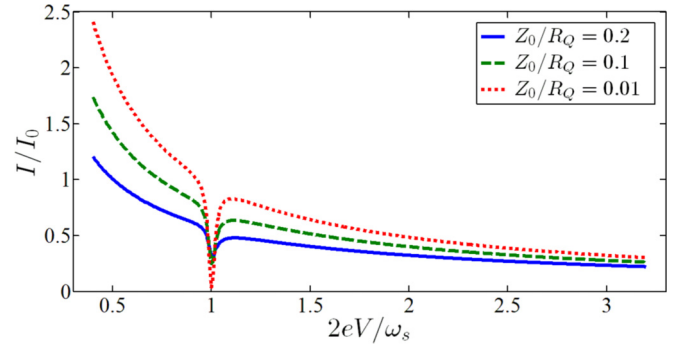

FIG. 2. (Color online) The linear regime: Current-voltage characteristic of the probe Josephson junction when placed at $m = 0$. The parameters are $\Gamma/\omega_s = 0.02$, $E_{\text{cut-off}}/\omega_s = 20$, and different Z_0 ($Z_0/R_Q = 0.01, 0.1, 0.2$). The side-coupled Josephson junction causes a resonance at $2eV = \omega_s$. In the limit $Z_0/R_Q \to 0$, the current vanishes at the resonance.

the scatterer modulates the phase difference between incoming and reflected photons and, thus, creates an interference pattern.

B. Current-voltage characteristic

To compute the current-voltage characteristic, we need to determine $P(E)$. This can be done numerically using the integral equation [33]

$$E P(E) = 2\int_0^E dE'\frac{\text{Re}[Z(E - E')]}{R_Q}P(E'). \quad (16)$$

The result can be obtained by starting with an arbitrary value $P(0)$ and then using the normalization condition $\int_0^{E_{\text{cut-off}}} P(E)dE = 1$, where $E_{\text{cut-off}} \gg \omega_s$.

The current-voltage characteristic is plotted in Fig. 2 for several values of the impedance of the transmission line. The characteristic current is given by

$$I_0 = \frac{\pi e(E_J^p)^2}{\omega_s}\frac{Z_0}{R_Q}. \quad (17)$$

The background current decreases with increasing voltage. In addition, there is a clear resonance feature at $2eV = \omega_s$.

This result can be understood as follows. The starting point is to recognize that when a bias voltage V is applied, Cooper pairs can flow through the probe junction provided that they can release their energy by emitting one or several photons into the environment.

First, let us concentrate on the regime $Z_0/R_Q \ll 1$. In that case, multiphoton processes are suppressed, and we can expand $e^{J(t)} \simeq 1 + J(t)$. Thus, the current is proportional to the Fourier transform of $J(t)$ at frequency $2eV$. It is straightforward to show that for a constant impedance this yields a current that decays with increasing voltage as $I(V) \propto 1/V$. On top of this, the resonance in the impedance at ω_s due to the side-coupled Josephson junction leads to a resonance in the current-voltage characteristic at $2eV = \omega_s$. Namely, the correction to the current $\delta I_1(\delta V)$ at voltages $V = \omega_s/(2e) + \delta V$ takes the form

$$\frac{\delta I_1(\delta V)}{I_0} = \frac{-\Gamma^2}{(2e\delta V)^2 + \Gamma^2}\left(\cos\alpha - \frac{2e\delta V}{\Gamma}\sin\alpha\right), \quad (18)$$
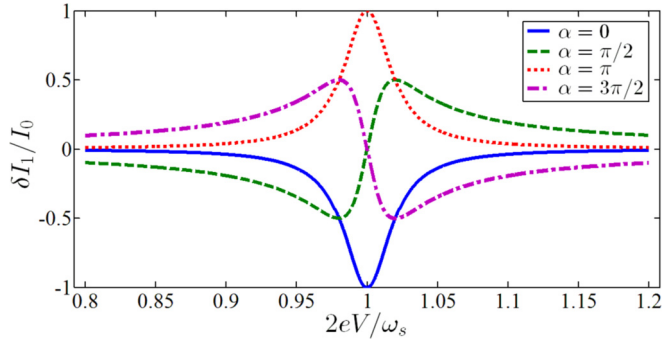
FIG. 3. (Color online) The resonance in the current-voltage characteristic for different values of the distance between the side-coupled Josephson junction and the probe Josephson junction, $\alpha = 2m\omega_s/\omega_0$. Results in the single-photon, linear regime are plotted [Eq. (18)] with $\Gamma/\omega_s = 0.02$. Note the effect of interference on the shape of the resonance.

where $\alpha = 2m\omega_s/\omega_0$. This leads to a complete extinction of the current at $\delta V = 0$ (at the one-photon level) when the probe is coupled to the same node as the side-coupled Josephson junction ($m = 0$). The shape of the resonance for different α is shown in Fig. 3; note the sensitivity to the placement of the probe produced by interference effects. The width of the resonance is given by $W_1 = \Gamma/e$, where Γ is given in Eq. (13).

Let us now turn to multiphoton processes corresponding to higher order terms in $J(t)$. These processes modify the resonance at $2eV = \omega_s$. In particular, while the scattering from the side-coupled Josephson junction may completely block the single-photon process at that voltage, this is not the case for the multiphoton processes: at most one photon can be on resonance, whereas the other photons will be off resonance and therefore propagate freely. Thus, the multiphoton processes lead to a finite current at the resonance. As an n-photon process yields a current contribution proportional to $(Z_0/R_Q)^n$, the

resonant structure weakens with increasing Z_0/R_Q due to the increasing importance of multiphoton processes.

In addition, one might expect that multiphoton processes lead to higher order resonances at voltages $2eV = n\omega_s$ ($n \geqslant 2$). We find, however, that this is not the case. While $2eV = n\omega_s$ is indeed a resonance condition for an n-photon process, the nonresonant background from the entire frequency range is large enough to completely overwhelm that contribution.

Thus, in the linear regime where photons do not interact, the side-coupled Josephson junction leads to a single resonance in the current voltage characteristic at $2eV = \omega_s$. As we will show below, additional features at $2eV = n\omega_s$ with $n \geqslant 2$ are a signature of photon-photon interactions.

IV. THE NONLINEAR REGIME

To investigate photon-photon interactions, we now take into account the nonlinearity of the side-coupled Josephson junction. In particular, we concentrate on the case of weak nonlinearity in the regime $E_J^s \gg e^2/(2C_\Sigma)$. To do so, we expand Eq. (3) up to fourth order in ϕ_δ,

$$H_J \approx H_J^{(0)} + V, \tag{19}$$

where

$$V = -\frac{E_J^s}{24}\phi_\delta^4. \tag{20}$$

In the following, we treat V as a perturbation.

A. Phase-phase correlator

As the Hamiltonian $H_{\text{nl}} \doteq H^{(0)} + V$ describes an interacting system, we can no longer write a closed form expression for the phase-phase correlator (6) in terms of $\langle \phi_n(t)\phi_m(0)\rangle$. Instead we expand (6) in powers of ϕ_m as follows:

$$\langle e^{i\phi_m(t)}e^{-i\phi_m(0)}\rangle_{H_{\text{nl}}} = 1 + \langle[\phi_m(t) - \phi_m(0)]\phi_m(0)\rangle_{H_{\text{nl}}} + \frac{1}{4}\langle[\phi_m^2(t) - \phi_m^2(0)]\phi_m^2(0)\rangle_{H_{\text{nl}}}$$
$$- \frac{1}{6}\{\langle[\phi_m^3(t) - \phi_m^3(0)]\phi_m(0)\rangle_{H_{\text{nl}}} + \langle[\phi_m(t) - \phi_m(0)]\phi_m^3(0)\rangle_{H_{\text{nl}}}\} + O(\phi_m^6). \tag{21}$$

Here the two-point phase-phase correlator represents single-photon processes, whereas the four-point phase-phase correlators represent two-photon processes. As before, we will use Green's functions to evaluate the correlators. In addition to the two-point Green's function $G_R(\phi_m,\phi_m;\omega)$, we now also need the four-point Green's functions $G_R(\phi_m^2,\phi_m^2;\omega)$, $G_R(\phi_m^3,\phi_m;\omega)$, and $G_R(\phi_m,\phi_m^3;\omega)$. In order to facilitate doing perturbation theory in the interaction V, we switch to imaginary-time-ordered or Matsubara Green's functions, $\mathscr{G}$.

Let us first evaluate the two-point Green's function $\mathscr{G}[\phi_n(\tau)\phi_m(0)]$, corresponding to single-photon processes. As shown in Appendix B, using the Dyson equation, we can sum up the perturbation series to all orders in the interactions. The representation in terms of Feynman diagrams is shown in Fig. 4. For the corresponding retarded Green's function

$G_R(\phi_n,\phi_m;\omega)$, we finally obtain

$$G_R(\phi_n,\phi_m;\omega) = G_R^{(0)}(\phi_n,\phi_m;\omega)$$
$$+ \frac{G_R^{(0)}(\phi_n,\phi_\delta;\omega)\frac{E_J^s}{2}\langle\phi_\delta^2\rangle_{H^{(0)}}G_R^{(0)}(\phi_\delta,\phi_m;\omega)}{1 - \frac{E_J^s}{2}\langle\phi_\delta^2\rangle_{H^{(0)}}G_R^{(0)}(\phi_\delta,\phi_\delta;\omega)}, \tag{22}$$

FIG. 4. (Color online) Dyson equation for the two-point Green's function. The nonlinearity results in a self-energy, $\Sigma = E_J^s\langle\phi_\delta^2\rangle_{H^{(0)}}/2$.

where $G_R^{(0)}$ is the Green's function in the absence of interactions.

Using the Green's functions $G_R^{(0)}$ and $\langle \phi_\delta^2 \rangle_{H^{(0)}}$ derived in Appendix A, we find that the local Green's function preserves its form though with a shifted resonance frequency ω_s'. Namely,

$$G_R(\phi_m, \phi_m; \omega) = i \frac{\pi}{\omega} \frac{Z_0}{R_Q} \left[1 + r'(\omega) e^{2i \frac{\omega}{\omega_0} m} \right], \qquad (23)$$

where

$$r'(\omega) = -\left[1 - 2i \frac{\omega_0}{\omega} \left(1 + \frac{C_0 C_\Sigma}{C_c^2} \frac{\omega^2 - \omega_s'^2}{\omega^2} \right) \right]^{-1} \qquad (24)$$

with $\omega_s' \approx \omega_s [1 - \omega_s/(8E_J^s)]$. In the same way, we can show that this is true for all two-point Green's functions. Note that $\delta \omega_s = \omega_s^2/(8E_J^s) \ll \omega_s$ coincides with the shift of the excitation energy between the ground and first excited states of the Hamiltonian (19).

Next we turn to the four-point Green's functions, corresponding to two-photon processes. Using perturbation theory, we may express them in terms of the two-point Green's functions. As we saw above, it is essential to sum up the perturbation series to all orders in V to obtain these two-point
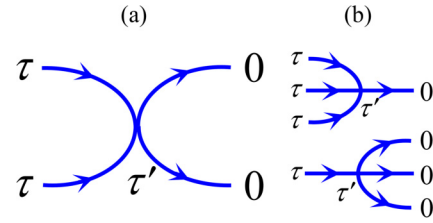

FIG. 5. (Color online) The Feynman diagrams for the interaction correction to the four-point Green's functions. (a) $\delta \mathscr{G}^{\text{int}}[\phi_n^2(\tau)\phi_m^2(0)]$. (b) $\mathscr{G}[\phi_n^3(\tau)\phi_m(0)]$ and $\mathscr{G}[\phi_n^3(\tau)\phi_m(0)]$.

Green's functions. By contrast, we will keep only the lowest order term in V accounting for interactions between the two photons. Then, the four-point Green's function $G_R(\phi_n^2, \phi_m^2; \omega)$ has two contributions: the first one describes the independent propagation of the two photons, whereas the second one describes the interaction effects. More precisely, the imaginary-time-ordered four-point Green's function may be written as $\mathscr{G}[\phi_n^2(\tau)\phi_m^2(0)] = \mathscr{G}^2[\phi_n(\tau)\phi_m(0)] + \delta \mathscr{G}^{\text{int}}[\phi_n^2(\tau)\phi_m^2(0)]$ with

$$\delta \mathscr{G}^{\text{int}} \left[\phi_n^2(\tau)\phi_m^2(0) \right]$$
$$\simeq E_J^s \int_0^\infty d\tau' \, \mathscr{G}^2[\phi_n(\tau)\phi_\delta(\tau')] \mathscr{G}^2[\phi_\delta(\tau')\phi_m(0)]. \qquad (25)$$

The corresponding Feynman diagram is shown in Fig. 5(a). The expression for the local retarded Green's function at zero temperature reads (see Appendix C)

$$\delta G_R^{\text{int}} \left(\phi_m^2, \phi_m^2; \omega \right) \simeq \frac{E_J^s}{\pi^2} \left(\sum_\pm \int_0^\infty d\omega_1 \, \text{Im}[G_R(\phi_m, \phi_\delta; \omega_1)] G_R(\phi_m, \phi_\delta; \omega \pm \omega_1) \right)^2. \qquad (26)$$

The leading order term for the other four-point Green's functions $G_R(\phi_n^3, \phi_m; \omega)$ and $G_R(\phi_n, \phi_m^3; \omega)$ is linear in E_J^s. In particular, we find the local Green's functions

$$G_R \left(\phi_m^3, \phi_m; \omega \right) \simeq \frac{E_J^s}{\pi^2} G_R(\phi_\delta, \phi_m; \omega) \int_0^\infty d\omega_1 \int_0^\infty d\omega_2 \, \text{Im}[G_R(\phi_m, \phi_\delta; \omega_1)] \text{Im}[G_R(\phi_m, \phi_\delta; \omega_2)] \sum_{s_1, s_2 = \pm} G_R(\phi_m, \phi_\delta; \omega + s_1 \omega_1 + s_2 \omega_2)$$

$$(27)$$

and $G_R(\phi_m, \phi_m^3; \omega) = G_R(\phi_m^3, \phi_m; \omega)$. The Feynman diagrams for the corresponding time-ordered Green's functions are shown in Fig. 5(b).

With the above results we can now write the phase-phase correlator needed to compute $P(E)$ in the following form:

$$\langle e^{i\phi_m(t)} e^{\phi_m(0)} \rangle_{H_{\text{nl}}} \simeq e^{J'(t)} + \delta J^{\text{int}}(t) \qquad (28)$$

with

$$J'(t) = \frac{1}{\pi} \int_0^\infty d\omega \, \text{Im}[G_R(\phi_m, \phi_m; \omega)](e^{-i\omega t} - 1), \quad (29)$$

$$\delta J^{\text{int}}(t) \simeq \frac{1}{\pi} \int_0^\infty d\omega \left\{ \frac{1}{4} \text{Im}[\delta G_R^{\text{int}}(\phi_m^2, \phi_m^2; \omega)] \right.$$
$$\left. - \frac{1}{3} \text{Im}[G_R(\phi_m^3, \phi_m; \omega)] \right\} (e^{-i\omega t} - 1). \qquad (30)$$

B. Current-voltage characteristic

Using Eq. (28) to compute $P(E)$, we obtain the current

$$I(V) \simeq e(E_J^p)^2 \left\{ \frac{1}{2} \int_{-\infty}^\infty dt \exp[i2eVt + J'(t)] \right.$$
$$+ \frac{1}{4} \text{Im}[\delta G_R^{\text{int}}(\phi_m^2, \phi_m^2; 2eV)]$$
$$\left. - \frac{1}{3} \text{Im}[G_R(\phi_m^3, \phi_m; 2eV)] \right\}. \qquad (31)$$

The first line describes the resonant structure discussed in Sec. III. Here the only effect of the nonlinearity is to shift the resonance from ω_s to ω_s'. The second line describes interaction effects between two photons. The current-voltage characteristic including these effects is shown in Fig. 6: it displays additional structure at $2eV = 2\omega_s'$.

The new peak at $2eV = 2\omega_s'$ comes from the contribution $\sim \delta G_R^{\text{int}}(\phi_m^2, \phi_m^2; 2eV)$. This contribution describes a process
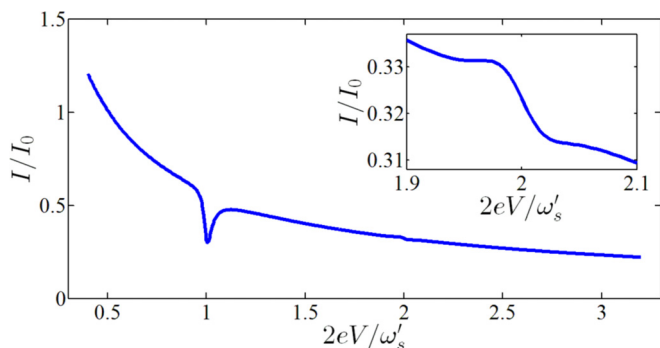
FIG. 6. (Color online) The nonlinear regime: Current-voltage characteristic of the probe Josephson junction when placed at $m = 0$. The parameters are $\omega_s'/E_J^s = 0.9$, $\Gamma/\omega_s' = 0.02$, $E_{\text{cut-off}}/\omega_s' = 20$, and $Z_0/R_Q = 0.2$. Photon-photon interactions lead to a second resonant feature at $2eV = 2\omega_s'$. A zoom on that feature with amplitude $\delta I_2/I_0 \propto (Z_0/R_Q)(\omega_s'/E_J^s)$ is shown in the inset.

in which a Cooper pair tunnels through the probe Josephson junction emitting two photons. When both photons are on resonance with the side-coupled Josephson junction, they interact strongly. This happens when each photon takes away half of the energy of the Cooper pair, $\omega = eV \simeq \omega_s'$. The resulting correction to the current is obtained using Eq. (26). As shown in Appendix C, for voltages $V = \omega_s'/e + \delta V$, it takes the form

$$\delta I_2(\delta V) = -I_0 \frac{\pi}{32} \frac{Z_0}{R_Q} \frac{\omega_s'}{E_J^s} \frac{\Gamma^2}{[(e\delta V)^2 + \Gamma^2]^2}$$
$$\times \left\{ \Gamma e \delta V \cos(2\alpha') - \frac{1}{2}[(e\delta V)^2 - \Gamma^2] \sin(2\alpha') \right\}, \quad (32)$$

where $\alpha' = 2m\omega_s'/\omega_0$.

The characteristic amplitude A_2 of the change in current is, thus, much smaller than I_0 or the single-photon resonant structure δI_1,

$$A_2 = \frac{\pi}{64} \frac{Z_0}{R_Q} \frac{\omega_s'}{E_J^s} I_0 \ll I_0. \quad (33)$$

Here, the suppression factor Z_0/R_Q is due to the fact that it is a two-photon process, whereas the suppression factor ω_s'/E_J^s is due to the fact that it is an interaction effect. Notice that the widths of the resonances at $2eV = \omega_s'$ and $2eV = 2\omega_s'$ are the same. The dependence of the shape of the second resonance on the distance $\propto \alpha'$ between the side-coupled Josephson junction and the probe Josephson junction is shown in Fig. 7.

We finally consider the current contribution stemming from $G_R(\phi_m^3, \phi_m; \omega)$. While it is in principle of the same order as the current contribution from $\delta G_R^{\text{int}}(\phi_m^2, \phi_m^2; \omega)$, i.e., it is proportional to $(Z_0/R_Q)(\omega_s'/E_J^s)I_0$, in this case it is impossible to fulfill the resonance condition simultaneously for all the photons involved. Therefore, this contribution acquires an additional suppression factor Γ/ω_s', and we can neglect it.

The main interaction effect is, thus, the appearance of a resonance at $2eV = 2\omega_s'$ due to two-photon processes. Higher order processes are expected to lead to additional features at $2eV = n\omega_s'$ ($n \geqslant 3$). However, their amplitude decreases rapidly with increasing n and may be estimated as $A_n \sim [(Z_0/R_Q)(\omega_s'/E_J^s)]^{n-1}I_0 \ll A_2$.
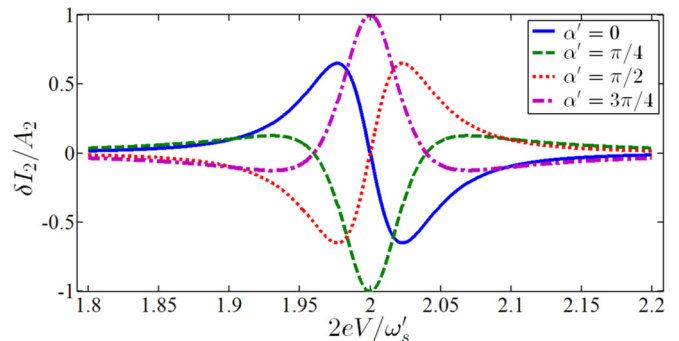

FIG. 7. (Color online) The second resonance in the current-voltage characteristic for different values of the distance between the side-coupled Josephson junction and the probe Josephson junction, $\alpha' = 2m\omega_s'/\omega_0$. Results are plotted near $2eV = 2\omega_s'$ in the two-photon, nonlinear regime [Eq. (32)] with $\Gamma/\omega_s' = 0.02$.

Taking typical parameters for realistic systems, we may estimate the amplitude A_2. While the Josephson energy E_J and the mutual capacitance C of a junction depend mainly on the junction area and, thus, cannot be varied independently, the capacitance to ground C_0 depends on the geometry and is therefore tunable. In the regime $C_0 \gg C$, the requirement $Z \lesssim R_Q$ limits the critical current and, by consequence, also the signal. We estimate that A_2 would be on the order of pA, making the effect accessible experimentally. A larger signal is expected in the opposite regime $C \gg C_0$, where one could use junctions with a much larger critical current. In this regime, the interaction between the side-coupled Josephson junction and the chain becomes nonlocal. This would make the theoretical analysis somewhat more complicated, but we expect that the results would not change qualitatively.

V. CONCLUSION

We have shown that the dc current-voltage characteristic of a Josephson junction provides a sensitive probe to study photon-photon interactions in a nonlinear environment. In particular, we investigated the case of a transmission line side-coupled to another Josephson junction whose nonlinearity leads to local photon-photon interactions. Scattering of individual photons by the side-coupled Josephson junction results in a resonance feature in the current-voltage characteristic of the probe Josephson junction at $2eV = \omega_s'$, where ω_s' is the plasma frequency of the side-coupled Josephson junction. By contrast, the interactions due to the nonlinearity yield an additional resonance feature at $2eV = 2\omega_s'$ due to two-photon processes. Such a feature is thus a clear indication of photon-photon interactions. While we concentrated here on the regime of a weak nonlinearity, it will be interesting to see how these features are modified in the strongly nonlinear regime.

APPENDIX A: TWO-POINT RETARDED GREEN'S FUNCTIONS

In this appendix, we derive the two-point retarded Green's functions $G_R^{(0)}$ of the linear system using equations of motion and scattering theory.

We start with the coupled equations of motion for $G_R^{(0)}(\phi_n, \phi_m; \omega)$ and $G_R^{(0)}(\phi_\delta, \phi_m; \omega)$,

$$\omega^2 G_R^{(0)}(\phi_n, \phi_m; \omega) - \omega_0^2 \left(1 + \frac{C_c^2}{C_0 C_\Sigma} \delta_{n0}\right)\left[2G_R^{(0)}(\phi_n, \phi_m; \omega) - G_R^{(0)}(\phi_{n+1}, \phi_m; \omega) - G_R^{(0)}(\phi_{n-1}, \phi_m; \omega)\right]$$

$$- \frac{C_c}{C_0}\omega_s^2 G_R^{(0)}(\phi_\delta, \phi_m; \omega)\delta_{n0} + \frac{(2e)^2}{C_0}\delta_{nm} = 0, \tag{A1}$$

$$(\omega^2 - \omega_s^2) G_R^{(0)}(\phi_\delta, \phi_m; \omega) - \frac{C_c}{C_\Sigma}\omega_0^2\left[2G_R^{(0)}(\phi_0, \phi_m; \omega) - G_R^{(0)}(\phi_1, \phi_m; \omega) - G_R^{(0)}(\phi_{-1}, \phi_m; \omega)\right] = 0. \tag{A2}$$

Combining Eqs. (A1) and (A2) then yields the following equation for $G_R^{(0)}(\phi_n, \phi_m; \omega)$,

$$\omega^2 G_R^{(0)}(\phi_n, \phi_m; \omega) - \omega_0^2\left(1 + \frac{C_c^2}{C_0 C_\Sigma}\frac{\omega^2}{\omega^2 - \omega_s^2}\delta_{n0}\right)\left[2G_R^{(0)}(\phi_n, \phi_m; \omega) - G_R^{(0)}(\phi_{n+1}, \phi_m; \omega) - G_R^{(0)}(\phi_{n-1}, \phi_m; \omega)\right] = -\frac{(2e)^2}{C_0}\delta_{nm}. \tag{A3}$$

If there is no side-coupling, $C_c = 0$, Eq. (A3) describes photons propagating freely along the infinite transmission line. At frequencies $\omega \ll \omega_0$, the dispersion is linear, $\omega = \omega_0 k$ with wave vector $k \ll 1$, and the solution is

$$G_{R,\,\mathrm{chain}}^{(0)}(\phi_n, \phi_m; \omega) = i\frac{\pi}{\omega}\frac{Z_0}{R_Q}e^{ik|n-m|}. \tag{A4}$$

The side-coupling leads to scattering of photons at the node $n = 0$. Then, for $m > 0$, the solution may be written in the form

$$G_R^{(0)}(\phi_n, \phi_m; \omega) = \begin{cases} Ae^{ikn} & n > m, \\ B[e^{-ikn} + r(\omega)e^{ikn}] & 0 < n < m, \\ Bt(\omega)e^{-ikn} & n < 0, \end{cases} \tag{A5}$$

where the reflection and transmission coefficients, $r(\omega)$ and $t(\omega)$, as well as the amplitudes A and B have to be determined using the boundary conditions at $n = 0$ and $n = m$. One finds $t(\omega) = 1 + r(\omega)$ with $r(\omega)$ given by Eq. (11) in the main text. Furthermore,

$$B = i\frac{\pi}{\omega}\frac{Z_0}{R_Q}e^{ikm}, \tag{A6}$$

$$A = B[e^{-2ikm} + r(\omega)]. \tag{A7}$$

The result is obtained by substituting Eqs. (11), (A6), and (A7) into Eq. (A5). Generalizing to arbitrary m, we find

$$G_R^{(0)}(\phi_n, \phi_m; \omega) = i\frac{\pi}{\omega}\frac{Z_0}{R_Q}[e^{ik|n-m|} + r(\omega)e^{ik(|n|+|m|)}]. \tag{A8}$$

The local Green's function needed to evaluate $P(E)$, thus, reads

$$G_R^{(0)}(\phi_m, \phi_m; \omega) = i\frac{\pi}{\omega}\frac{Z_0}{R_Q}[1 + r(\omega)e^{2ik|m|}]. \tag{A9}$$

While this is the only Green's function needed in the linear case, more Green's functions are required in the nonlinear case. Using Eq. (A2), we obtain

$$G_R^{(0)}(\phi_\delta, \phi_m; \omega) = -2\frac{\pi}{\omega}\frac{1}{R_Q C_c \omega}r(\omega)e^{ik|m|}. \tag{A10}$$

Similarly, the Green's functions $G_R^{(0)}(\phi_m, \phi_\delta; \omega)$ and $G_R^{(0)}(\phi_\delta, \phi_\delta; \omega)$ obey coupled equations of motion. One may show that $G_R^{(0)}(\phi_m, \phi_\delta; \omega) = G_R^{(0)}(\phi_\delta, \phi_m; \omega)$, whereas the equation for $G_R^{(0)}(\phi_\delta, \phi_\delta; \omega)$ is

$$(\omega^2 - \omega_s^2) G_R^{(0)}(\phi_\delta, \phi_\delta; \omega) - \frac{C_c}{C_\Sigma}\omega_0^2\left[2G_R^{(0)}(\phi_0, \phi_\delta; \omega) - G_R^{(0)}(\phi_1, \phi_\delta; \omega) - G_R^{(0)}(\phi_{-1}, \phi_\delta; \omega)\right] = -\frac{(2e)^2}{C_\Sigma}. \tag{A11}$$

Using Eq. (A10), one obtains

$$G_R^{(0)}(\phi_\delta, \phi_\delta; \omega) = -4i\frac{\pi}{\omega}\frac{1}{R_Q Z_0 (C_c \omega)^2}r(\omega). \tag{A12}$$

Using the explicit expression for $r(\omega)$, Eq. (A12) may be rewritten as

$$G_R^{(0)}(\phi_\delta, \phi_\delta; \omega) = -\frac{2\pi}{R_Q C_\Sigma}\frac{1}{\omega^2 - \omega_s^2 + i\frac{C_c^2}{2C_0 C_\Sigma}\frac{\omega^2}{\omega_0}(\omega - 2i\omega_0)}. \tag{A13}$$

Finally, using the fact that $C_c^2/(C_0 C_\Sigma) \ll 1$, we approximate

$$G_R^{(0)}(\phi_\delta, \phi_\delta; \omega) \simeq -\frac{2\pi}{R_Q C_\Sigma} \frac{1}{\omega^2 - (\omega_s - i\Gamma)^2}, \tag{A14}$$

where

$$\Gamma = \frac{1}{4} \frac{C_c^2}{C_0 C_\Sigma} \frac{\omega_s^2}{\omega_0}.$$

This result also allows us to evaluate

$$\langle \phi_\delta^2 \rangle_{H^{(0)}} = \frac{1}{\pi} \int_0^\infty d\omega \, \mathrm{Im}\big[G_R^{(0)}(\phi_\delta, \phi_\delta; \omega) \big] = \frac{\omega_s}{2 E_J^{\mathrm{s}}}. \tag{A15}$$

APPENDIX B: THE DYSON EQUATION

In the following, we present the derivation of Eq. (22).

The time-ordered two-point Green's function is defined as

$$\mathcal{G}[\phi_n(\tau)\phi_m(0)] = \langle T_\tau \phi_n(\tau)\phi_m(0) \rangle_{H_{\mathrm{nl}}}, \tag{B1}$$

where T_τ is the time-ordering operator. Equation (B1) can be rewritten as

$$\mathcal{G}[\phi_n(\tau)\phi_m(0)] = \frac{\langle T_\tau \phi_n(\tau)\phi_m(0) S(\infty) \rangle_{H^{(0)}}}{\langle S(\infty) \rangle_{H^{(0)}}}, \tag{B2}$$

where $S(\infty) = T_\tau \exp\left[-\int_0^\infty d\tau' \, V(\tau') \right]$.

Expanding Eq. (B2) up to first order in the perturbation $V = -E_J^{\mathrm{s}} \phi_\delta^4/24$ and using Wick's theorem yields

$$\mathcal{G}[\phi_n(\tau)\phi_m(0)] \simeq \mathcal{G}^{(0)}[\phi_n(\tau)\phi_m(0)] + \int_0^\infty d\tau' \mathcal{G}^{(0)}[\phi_n(\tau)\phi_\delta(\tau')] \frac{E_J^s}{2} \langle \phi_\delta^2 \rangle_{H^{(0)}} \mathcal{G}^{(0)}[\phi_\delta(\tau')\phi_m(0)]. \tag{B3}$$

After Fourier transformation and analytical continuation, one obtains the corresponding retarded Green's function,

$$G_R(\phi_n, \phi_m; \omega) \simeq G_R^{(0)}(\phi_n, \phi_m; \omega) + G_R^{(0)}(\phi_n, \phi_\delta; \omega) \frac{E_J^s}{2} \langle \phi_\delta^2 \rangle_{H^{(0)}} G_R^{(0)}(\phi_\delta, \phi_m; \omega). \tag{B4}$$

While far from the resonance at $\omega = \omega_s$ the second term is much smaller than the first one, this is no longer true close to the resonance. Thus, this first-order expansion is not sufficient is to describe the modifications to the resonance due to the perturbation. It is possible to go beyond the first-order expansion by realizing that $E_J^{\mathrm{s}} \langle \phi_\delta^2 \rangle_{H^{(0)}}/2$ is a local self-energy, $\Sigma(\phi_\delta, \phi_\delta)$. Thus, one obtains the Dyson equation

$$G_R(\phi_n, \phi_m; \omega) = G_R^{(0)}(\phi_n, \phi_m; \omega) + G_R^{(0)}(\phi_n, \phi_\delta; \omega) \frac{E_J^s}{2} \langle \phi_\delta^2 \rangle_{H^{(0)}} G_R(\phi_\delta, \phi_m; \omega), \tag{B5}$$

A similar equation can be written for the Green's function $G_R(\phi_\delta, \phi_m; \omega)$. Namely,

$$G_R(\phi_\delta, \phi_m; \omega) = G_R^{(0)}(\phi_\delta, \phi_m; \omega) + G_R^{(0)}(\phi_\delta, \phi_\delta; \omega) \frac{E_J^s}{2} \langle \phi_\delta^2 \rangle_{H^{(0)}} G_R(\phi_\delta, \phi_m; \omega). \tag{B6}$$

Combining Eqs. (B5) and (B6), we obtain the result

$$G_R(\phi_n, \phi_m; \omega) = G_R^{(0)}(\phi_n, \phi_m; \omega) + \frac{G_R^{(0)}(\phi_n, \phi_\delta; \omega) \frac{E_J^s}{2} \langle \phi_\delta^2 \rangle_{H^{(0)}} G_R^{(0)}(\phi_\delta, \phi_m; \omega)}{1 - \frac{E_J^s}{2} \langle \phi_\delta^2 \rangle_{H^{(0)}} G_R^{(0)}(\phi_\delta, \phi_\delta; \omega)}. \tag{B7}$$

Then, using the Green's functions $G_R^{(0)}$ of the linear problem derived in Appendix A, we find that the full Green's function $G_R(\phi_n, \phi_m; \omega)$ has the same form as $G_R^{(0)}(\phi_n, \phi_m; \omega)$ though with a shift of the resonance frequency, $\omega_s \to \omega_s' \approx \omega_s(1 - \langle \phi_\delta^2 \rangle_{H^{(0)}}/4)$. Similarly, we find that this frequency shift appears in all two-point Green's functions.

APPENDIX C: THE CONTRIBUTION OF PHOTON-PHOTON INTERACTION

The four-point retarded Green's function $\delta G_R^{\mathrm{int}}(\phi_m^2, \phi_m^2; \omega)$, needed to compute the interaction contribution to the current-voltage characteristic, is obtained from Eq. (25) by taking the Fourier transform and then performing the analytical continuation from Matsubara to real frequencies, $i\omega_\nu \to \omega + i0^+$, and using standard methods of contour integration. One obtains Eq. (26) which

takes the form $\delta G_R^{\text{int}}(\phi_m^2,\phi_m^2;\omega) \simeq (E_J^s/\pi^2) f^2(\omega)$, where

$$f(\omega) = \sum_{\pm} \int_0^{\infty} d\omega_1 \, \text{Im}[G_R(\phi_m,\phi_\delta;\omega_1)] G_R(\phi_m,\phi_\delta;\omega \pm \omega_1). \tag{C1}$$

The integral is dominated by frequencies where both Green's functions are close to resonance, $\omega_1 \approx \omega \pm \omega_1 \approx \omega_s'$. This requires $\omega \approx 2\omega_s'$. We, thus, approximate $\omega = 2\omega_s' + \delta\omega$ and $\omega_1 = \omega_s' + \delta\omega_1$. The Green's functions close to resonance take the form

$$G_R^{(0)}(\phi_\delta,\phi_m;\omega_s'+\delta\omega) \simeq 2\frac{\pi}{\omega_s'}\frac{1}{R_Q C_c \omega_s'}\frac{1}{1-i\frac{\delta\omega}{\Gamma}}e^{i\frac{\omega_s'}{\omega_0}|m|}. \tag{C2}$$

We then rewrite

$$f(\omega) \simeq \left(\frac{2\pi}{R_Q C_c (\omega_s')^2}\right)^2 e^{i\frac{\omega_s'}{\omega_0}|m|} \int_{-\infty}^{\infty} d\delta\omega_1 \, \frac{\sin\frac{\omega_s'|m|}{\omega_0} + \frac{\delta\omega_1}{\Gamma}\cos\frac{\omega_s'|m|}{\omega_0}}{1+\left(\frac{\delta\omega_1}{\Gamma}\right)^2}\frac{1}{1-i\frac{\delta\omega-\delta\omega_1}{\Gamma}}. \tag{C3}$$

It is straightforward to evaluate the convolution integrals to obtain

$$\text{Re}[f(\omega)] \simeq \pi\left(\frac{\pi C_c}{2R_Q C_0 C_\Sigma}\right)^2 \frac{\delta\omega\cos\alpha' + 2\Gamma\sin\alpha'}{(\delta\omega)^2 + 4\Gamma^2}, \tag{C4}$$

$$\text{Im}[f(\omega)] \simeq -\pi\left(\frac{\pi C_c}{2R_Q C_0 C_\Sigma}\right)^2 \frac{2\Gamma\cos\alpha' - \delta\omega\sin\alpha'}{(\delta\omega)^2 + 4\Gamma^2}. \tag{C5}$$

Finally, to compute the current-voltage characteristic, we need

$$\text{Im}\left[\delta G_R^{\text{int}}(\phi_m^2,\phi_m^2;2\omega_s'+\delta\omega)\right] \simeq \frac{2E_J^s}{\pi^2}\text{Re}\left[f(2\omega_s'+\delta\omega)\right]\text{Im}\left[f(2\omega_s'+\delta\omega)\right]$$

$$\simeq -\frac{\pi^2}{8}\frac{1}{E_J^s}\left(\frac{Z_0}{R_Q}\right)^2 \frac{4\Gamma^2}{[(\delta\omega)^2+4\Gamma^2]^2}\left\{2\delta\omega\Gamma\cos(2\alpha') - \frac{1}{2}\left(\delta\omega^2 - 4\Gamma^2\right)\sin(2\alpha')\right\}. \tag{C6}$$

[1] R. J. Schoelkopf and S. M. Girvin, Wiring up quantum systems, Nature (London) **451**, 664 (2008).

[2] Serge Haroche, Nobel lecture: Controlling photons in a box and exploring the quantum to classical boundary, Rev. Mod. Phys. **85**, 1083 (2013).

[3] David J. Wineland, Nobel lecture: Superposition, entanglement, and raising Schrödinger's cat, Rev. Mod. Phys. **85**, 1103 (2013).

[4] I. Carusotto and C. Ciuti, Quantum fluids of light, Rev. Mod. Phys. **85**, 299 (2013).

[5] T. E. Northup and R. Blatt, Quantum information transfer using photons, Nat. Photonics **8**, 356 (2014).

[6] Nicolas Gisin and Rob Thew, Quantum communication, Nat. Photonics **1**, 165 (2007).

[7] S. Haroche and J.-M. Raimond, *Exploring the Quantum* (Oxford University Press, Oxford, 2006).

[8] Io-Chun Hoi, C. M. Wilson, Göran Johansson, Joel Lindkvist, Borja Peropadre, Tauno Palomaki, and Per Delsing, Microwave quantum optics with an artificial atom in one-dimensional open space, New J. Phys. **15**, 025011 (2013).

[9] A. F. van Loo, A. Fedorov, K. Lalumiere, B. C. Sanders, A. Blais, and Andreas Wallraff, Photon-mediated interactions between distant artificial atoms, Science **342**, 1494 (2013).

[10] Marijn A. M. Versteegh, Michael E. Reimer, Klaus D. Jöns, Dan Dalacu, Philip J. Poole, Angelo Gulinatti, Andrea Giudice, and Val Zwiller, Observation of strongly entangled photon pairs from a nanowire quantum dot, Nat. Commun. **5**, 5298 (2014).

[11] M. Arcari, I. Söllner, A. Javadi, S. Lindskov Hansen, S. Mahmoodian, J. Liu, H. Thyrrestrup, E. H. Lee, J. D. Song, S. Stobbe, and P. Lodahl, Near-Unity Coupling Efficiency of a Quantum Emitter to a Photonic Crystal Waveguide, Phys. Rev. Lett. **113**, 093603 (2014).

[12] E. Vetsch, D. Reitz, G. Sagué, R. Schmidt, S. T. Dawkins, and A. Rauschenbeutel, Optical Interface Created by Laser-Cooled Atoms Trapped in the Evanescent Field Surrounding an Optical Nanofiber, Phys. Rev. Lett. **104**, 203603 (2010).

[13] Sanli Faez, Pierre Türschmann, Harald R. Haakh, Stephan Götzinger, and Vahid Sandoghdar, Coherent Interaction of Light and Single Molecules in a Dielectric Nanoguide, Phys. Rev. Lett. **113**, 213601 (2014).

[14] A. LeClair, F. Lesage, S. Lukyanov, and H. Saleur, The Maxwell-Bloch theory in quantum optics and the Kondo model, Phys. Lett. A **235**, 203 (1997).

[15] Jung-Tsung Shen and Shanhui Fan, Strongly Correlated Two-Photon Transport in a One-Dimensional Waveguide Coupled to a Two-Level System, Phys. Rev. Lett. **98**, 153003 (2007).

[16] Huaixiu Zheng, Daniel J. Gauthier, and Harold U. Baranger, Waveguide QED: Many-body bound-state effects in coherent and Fock-state scattering from a two-level system, Phys. Rev. A **82**, 063816 (2010).

[17] Karyn Le Hur, Kondo resonance of a microwave photon, Phys. Rev. B **85**, 140506(R) (2012).

[18] M. Goldstein, M. H. Devoret, M. Houzet, and L. I. Glazman, Inelastic Microwave Photon Scattering off a Quantum Impurity in a Josephson-Junction Array, Phys. Rev. Lett. **110**, 017002 (2013).

[19] Stojan Rebić, Jason Twamley, and Gerard J. Milburn, Giant Kerr Nonlinearities in Circuit Quantum Electrodynamics, Phys. Rev. Lett. **103**, 150503 (2009).

[20] S. Bera, S. Florens, H. U. Baranger, N. Roch, A. Nazir, and A. W. Chin, Stabilizing spin coherence through environmental entanglement in strongly dissipative quantum systems, Phys. Rev. B **89**, 121108(R) (2014).

[21] A. J. Leggett, S. Chakravarty, A. T. Dorsey, Matthew P. A. Fisher, Anupam Garg, and W. Zwerger, Dynamics of the dissipative two-state system, Rev. Mod. Phys. **59**, 1 (1987).

[22] Ulrich Weiss, *Quantum Dissipative Systems*, 4th ed. (World Scientific, Singapore, 2012).

[23] T. Niemczyk, F. Deppe, H. Huebl, E. P. Menzel, F. Hocke, M. J. Schwarz, J. J. Garcia-Ripoll, D. Zueco, T. Hümmer, E. Solano, A. Marx, and R. Gross, Circuit quantum electrodynamics in the ultrastrong-coupling regime, Nat. Phys. **6**, 772 (2010).

[24] P. Forn-Díaz, J. Lisenfeld, D. Marcos, J. J. García-Ripoll, E. Solano, C. J. P. M. Harmans, and J. E. Mooij, Observation of the Bloch-Siegert Shift in a Qubit-Oscillator System in the Ultrastrong Coupling Regime, Phys. Rev. Lett. **105**, 237001 (2010).

[25] R. M. Bradley and S. Doniach, Quantum fluctuations in chains of Josephson junctions, Phys. Rev. B **30**, 1138 (1984).

[26] N. A. Masluk, I. M. Pop, A. Kamal, Z. K. Minev, and M. H. Devoret, Microwave Characterization of Josephson Junction Arrays: Implementing a Low Loss Superinductance, Phys. Rev. Lett. **109**, 137002 (2012).

[27] M. T. Bell, I. A. Sadovskyy, L. B. Ioffe, A. Yu. Kitaev, and M. E. Gershenson, Quantum Superinductor with Tunable Nonlinearity, Phys. Rev. Lett. **109**, 137003 (2012).

[28] C. Altimiras, O. Parlavecchio, P. Joyez, D. Vion, P. Roche, D. Esteve, and F. Portier, Tunable microwave impedance matching to a high impedance source using a Josephson metamaterial, Appl. Phys. Lett. **103**, 212601 (2013).

[29] T. Weissl, G. Rastelli, I. Matei, I. M. Pop, O. Buisson, F. W. J. Hekking, and W. Guichard, Bloch band dynamics of a Josephson junction in an inductive environment, Phys. Rev. B **91**, 014507 (2015).

[30] Yu. Makhlin, G. Schön, and A. Schnirman, Quantum-state engineering with Josephson-junction devices, Rev. Mod. Phys. **73**, 357 (2001).

[31] V. Bouchiat, D. Vion, P. Joyez, D. Esteve, and M. H. Devoret, Quantum coherence with a single Cooper pair, Phys. Scr., **T76**, 165 (1998).

[32] Y. Nakamura, Y. A. Pashkin, and J. S. Tsai, Coherent control of macroscopic quantum states in a single-Cooper-pair box, Nature (London) **398**, 786 (1999).

[33] G.-L. Ingold and Yu. V. Nazarov, Charge tunneling rates in ultrasmall junctions, in *Single Charge Tunneling: Coulomb Blockade Phenomena in Nanostructures*, edited by H. Grabert and M. H. Devoret (Plenum, New York, 1992), p. 21.

[34] Tero T. Heikkilä, Pauli Virtanen, Göran Johansson, and Frank K. Wilhelm, Measuring Non-Gaussian Fluctuations through Incoherent Cooper-Pair Current, Phys. Rev. Lett. **93**, 247005 (2004).

[35] D. M. Basko and F. W. J. Hekking, Disordered Josephson junction chains: Anderson localization of normal modes and impedance fluctuations, Phys. Rev. B **88**, 094507 (2013).

[36] S. Jezouin, M. Albert, F. D. Parmentier, A. Anthore, U. Gennser, A. Cavanna, I. Safi, and F. Pierre, Tomonaga-Luttinger physics in electronic quantum circuits, Nat. Commun. **4**, 1802 (2013).

[37] Philippe Joyez, Self-Consistent Dynamics of a Josephson Junction in the Presence of an Arbitrary Environment, Phys. Rev. Lett. **110**, 217003 (2013).

[38] J.-R. Souquet, I. Safi, and P. Simon, Dynamical Coulomb blockade in an interacting one-dimensional system coupled to an arbitrary environment, Phys. Rev. B **88**, 205419 (2013).